PAPER

# The phonon-related effective Hamiltonian method for displacive ferroelectric materials

Electronic Structure

PAPER

# The phonon-related effective Hamiltonian method for displacive ferroelectric materials

RECEIVED
30 July 2019

REVISED
4 November 2019

ACCEPTED FOR PUBLICATION
18 November 2019

PUBLISHED
3 December 2019

Qi-Jun Ye[1], Xue-Feng Zhang[1] and Xin-Zheng Li[1,2]

[1] State Key Laboratory for Artificial Microstructure and Mesoscopic Physics, and School of Physics, Peking University, Beijing 100871, People's Republic of China

[2] Collaborative Innovation Center of Quantum Matter, Peking University, Beijing 100871, People's Republic of China

**E-mail:** xzli@pku.edu.cn

**Keywords:** effective Hamiltonian, ferroelectric, soft phonon mode, first principles derived method

## Abstract

In this manuscript, we explain the theoretical principles and some technical details of a first-principles derived effective Hamiltonian method, which is used to calculate the ferroelectric (FE) and structural properties in displacive FE materials. Exploiting that the key instabilities responsible for this phase transition are governed by soft phonons, this Hamiltonian is phonon-related, i.e. using phonon modes as variables and describing their intra- and interactions. Upon retaining the predictive power of first-principles calculations, this method is computationally cheap, which enables large supercell being used so that the thermodynamic limit can be reached easily in the simulations at finite temperatures. Besides the known success in perovskites, it also qualifies for characterizing FE phase transitions in the rocksalt type group-IV monochalcogenides, and shows potential applications in more complicated systems, e.g. M-type hexaferrite.

## 1. Introduction

The pursuit for high dielectric constant insulators and nonvolatile memories in semiconductor applications has stimulated studies of ferroelectric (FE) materials [1–7]. Nowadays, developments of the first-principles density-functional theory (DFT) methods mean that our theoretical understandings of the physics of FEs have reached a high level of accuracy in describing the electronic properties, reproducing experimental results, and even predicting novel materials [8–10]. In most of these DFT calculations, properties of the system were simulated using static nuclei at or close to the equilibrium structure, and the size of the supercells used was restricted to a few hundreds of (or at most one or two thousands of) atoms. Characteristic lengths of a realistic paraelectric (PE) to FE phase transition, however, require supercells to be much larger. Concerning statistics, long-time simulations were often needed to obtain thermal equilibrium properties. Therefore, despite the continuing advances of supercomputer, these requirements are still clearly beyond the scope of a direct first-principles simulation. Accurate first-principles derived models (the parameters are determined by first-principles calculations) are highly desired for predictive and atomic level studies of these problems at nonzero temperatures ($T$s).

In this manuscript, we focus on such effective Hamiltonian methods (also known as the model Hamiltonian methods). In the earliest attempts, a FE model is typically used to provide insights into the FE origin of materials. For example, the Landau phenomenological model interprets the formation of ordered state as a result of varied free energy surface from the high $T$ centered single well structure to the low $T$ symmetrized off-center double well structure [11, 12]. These empirical or experiment derived model are physically transparent. However, they often fail in predicting properties, e.g. phase transition temperature, quantitatively. The cost of simplicity is the omission of some crucial features of the real system. The temperature effects naturally appear as fluctuations upon the static energy profile, while in Landau model they are imposed by directly modifying the potential (the interaction coefficients are $T$ dependent). The $\phi^4$ model enhances intersite fluctuations, while the long-range interaction and the elastic coupling are still missing [11–13]. An improved model should resort to the predictive power of first-principles calculations. Besides, the variables in these models are artificial order parameters refined from macroscopic phenomena and experimental measurements, such as polarizations for FEs. One should construct

the model with variables originated from a microscopic level, such as atomic displacement patterns. The effective Hamiltonian serves in the features of both first-principles derived and phonon-related, would have a better performance.

In a different way from models, DFT derived force field could provide interaction details at the atomistic level [14]. These force fields allow molecular dynamics simulations with large system sizes and long-times to be performed with decent computational cost, to obtain the thermodynamic quantities of interest. However, these attempts cannot give rise to a clear physical picture. The distinctive characteristic have been hindered underneath the sophisticated parameters of these force fields. Indeed, the analysis of phonon spectrum demonstrates that only a subset of degrees of freedom (DOF), i.e. soft phonon mode (with imaginary frequencies, labeled as SM), is responsible for the key instabilities and subsequent phase transitions. Therefore, it's much smarter to focus on a few crucial collective modes rather than all of the separated atoms, and then construct a potential to parameterize the intra- and interaction of these modes. In so doing, the original atomic potential could be decomposed into two part: a leading part of SM and a regular part of hard phonon modes (with real frequencies, labeled as HM). It's essential to distinguish them. The showup of anharmonicity in the former highlights the treatments for terms of orders higher than harmonic, while the latter could be approximated as harmonic oscillators. The usage of soft phonon picture can capture the dominant characteristic and hence to a simplified potential and sensible explanations for the interaction details.

Achieving both the elegance of models and accuracy of DFT derived force field, the phonon related effective Hamiltonian method provides to be a good alternative. Since the early proposal by Vanderbilt *et al* [15–17], it has been witnessed competent in describing the FE and structural features of a series of perovskites [18–23]. In fact, the validity of effective Hamiltonian can be viewed from the preservation of partition function [24]. Typically for a *NVT* ensemble, the partition function is written as the integral over the phase space

$$Z_{NVT}^{\mathrm{ori}} = Z(\mathcal{H}^{\mathrm{ori}}) = \int \mathrm{d}^{3N} p_i \int \mathrm{d}^{3N} r_i \exp\left[-\beta \mathcal{H}^{\mathrm{ori}}(p_i, r_i)\right], \tag{1}$$

where $\{p_i\}$ and $\{r_i\}$ are conjugated momentum and position of $i$th DOF, respectively. The effective Hamiltonian is so-called since it satisfies

$$Z_{NVT}^{\mathrm{eff}} = Z(\mathcal{H}^{\mathrm{eff}}) = \int \mathrm{d}^{3M} p_i' \int \mathrm{d}^{3M} r_i' \exp\left[-\beta \mathcal{H}^{\mathrm{eff}}(p_i', r_i')\right] = Z(\mathcal{H}^{\mathrm{ori}})/A, \tag{2}$$

where the integrations are performed in a subspace with the new variables $\{p_i'\}$ and $\{r_i'\}$, and the subset of the other DOF are integrated out as $A$. Actually, $A$ represents for the approximations we made to derive $\mathcal{H}^{\mathrm{eff}}$ from $\mathcal{H}^{\mathrm{ori}}$. It relates very close with the partition function of the integrated DOFs which we would explain in details later. Here, $\{p_i'\}$ and $\{r_i'\}$ can be linear combination of the original sets or of its part. Noted that in so doing, the DOF have also decreased to $3M \leqslant 3N$, which indicates a simpler picture retaining original statistical results. The convenience in the choice of variables enables a direct observation of the interested order parameters. For one observable $B$ which could be expressed in formula of microscopic variables, the original and effective Hamiltonian gives the same statistical results

$$\langle B(\{p_i\}, \{r_i\})\rangle_{Z^{\mathrm{ori}}} = \langle B(\{p_i'\}, \{r_i'\})\rangle_{Z^{\mathrm{eff}}}. \tag{3}$$

Since the partition function can produce the required statistical quantities in representation of the new phase space, the question comes to:

- The choice of variables. Rather than a full configuration space used by atomic interaction force field, we want to choose only a subspace of the variables in constructing the effective Hamiltonian. Simplicity and expansibility are the key factors which should be considered in choosing such a subset of DOF.
- The connection of used variables to observations. Are the phonon related variable (typically the coordinates of particles or their linear combinations) capable of describing the FE properties of FE materials?

In the following, we will present the construction of the effective Hamiltonian with variables chosen as the magnitude of the local soft phonon modes and lattice strains. All the approximations and considerations used to derive the final formula from the original Hamiltonian of solids, are explained in details. A general implementation procedure is sketched, and some material-specific examples are given later. These examples include our simulations of the phase transitions in the 3D bulk and the 2D layers of SnTe, as well as some potential applications in a more complicated displacive FE material, i.e. hexaferrite.

## 2. Theoretical derivation

### 2.1. Phonon-related Hamiltonian

We shall start with the many-body Hamiltonian of solids. For a conventional solids, the Hamiltonian consists of intra- and interaction between nuclei and electrons, as

$$\mathcal{H}_{\rm tot} = T_{\rm n} + V_{\rm n-n}(\{R_I\}) + T_{\rm e} + V_{\rm e-e}(\{r_i\}) + V_{\rm n-e}(\{R_I\},\{r_i\}), \tag{4}$$

where $\{R_I\}$ and $\{r_i\}$ represents the positions of nuclei and electrons, respectively. Retaining to well-known Born–Oppenheimer approximation, it can be simplified by separating the dependence of nuclei and electrons, as

$$\mathcal{H}^{\rm eff}_{{\rm e},\{R_I\}} = T_{\rm e} + V_{\rm e-e}(\{r_i\}) + V_{\rm n-e}(\{R_I\},\{r_i\}), \tag{5}$$

$$\mathcal{H}^{\rm eff}_{\rm n} = T_{\rm n} + V_{\rm n-n}(\{R_I\}) + E_{\rm n-e}(\{R_I\}), \tag{6}$$

where equation (5) is solved with frozen nuclear positions. It is the subject of many-body electronic structure theory, e.g. DFT calculations. Solution of this equation (5) then gives the $E_{\rm n-e}(\{R_I\})$ as an input in equation (6). Since the integration of the kinetic energy in the partition function is always a constant (subjected to the condition that the potential energy is conservative, which is respected in this case), only the effective potential energy

$$V^{\rm eff}_{\rm n} = V_{\rm n-n}(\{R_I\}) + E_{\rm n-e}(\{R_I\}) \tag{7}$$

will be considered. As such, we focus on the nuclear part and integrate out the DOF of electrons. Once the electronic properties can be estimated in formula of nuclear coordinates, the corresponding observation will be gained from a nuclear effective Hamiltonian. Though such maps may not be established or found for all electronic properties, the polarizations in displacive FE materials meets this requirement. This Hamiltonian could reproduce equivalent statistical results in phonon-related properties refraining from computationally consuming DFT calculation.

We choose to expand the potential energy by Taylor series in atomic displacements from the reference structure, regarding the nature for solids that atoms are oscillating around their equilibrium positions. The translational symmetry is naturally conserved by doing so, since the Hamiltonian now relies on relative positions instead of the absolute ones. The reference structure for one FE material is usually chose to be the structure corresponding to high $T$, whose high symmetry would help us to simplify the interaction formula by requiring less parameters. As mentioned, the collective displacement pattern (phonon modes) are more suitable descriptors than the separated atomic displacements. We characterize these phonon modes in the reciprocal space. The potential energy is written out in the formula of phonon modes, as

$$V_{\rm n} = \sum_{\boldsymbol{\xi}_{\mathbf{k},s}} V^{(1)}(\boldsymbol{\xi}_{\mathbf{k},s}) + \sum_{\boldsymbol{\xi}_{\mathbf{k},s}} {\sum_{\boldsymbol{\xi}_{\mathbf{k}',s'}}}' V^{(2)}(\boldsymbol{\xi}_{\mathbf{k},s},\boldsymbol{\xi}_{\mathbf{k}',s'}) + \cdots, \tag{8}$$

where $\boldsymbol{\xi}_{\mathbf{k},s}$ labels the $s$th phonon mode with the reciprocal vector $\mathbf{k}$. $V^{(i)}$ represents the $i$-body interactions among phonons, and the prime in two-body summation means that $(\mathbf{k},s)$ and $(\mathbf{k}',s')$ must not be same. For the displacive FE materials, the phonon modes of the reference structure could be distinguished into soft modes (SM) and the other hard modes (HM), depending on whether the corresponding spring constant is smaller than zero or not, as the subspace of the soft modes

$$\Omega^{\rm SM} := \left\{ \xi^{\rm SM}_{\mathbf{k},s} \;\middle|\; [\omega(\mathbf{k},s)]^2 < 0 \right\} \tag{9}$$

and the subspace of the hard modes

$$\Omega^{\rm HM} := \left\{ \xi^{\rm HM}_{\mathbf{k},s} \;\middle|\; [\omega(\mathbf{k},s)]^2 \geqslant 0 \right\}. \tag{10}$$

Keeping up to two-body terms, the Hamiltonian is split as

$$V_{\rm n} \approx V^{(1)}_{\rm SM} + V^{(1)}_{\rm HM} + V^{(2)}_{\rm SM-SM} + V^{(2)}_{\rm SM-HM} + V^{(2)}_{\rm HM-HM}, \tag{11}$$

where the first two terms are for one-body terms of SM and HM, and the last three summations are for two-body terms between different SMs, different HMs, and HM and SM, respectively. Soft modes indicate the emerged instabilities of the materials, e.g. FE soft modes describe the instabilities for system going from high-symmetry PE phase to symmetry-breaking FE phase. In the light of order parameters in Landau model, soft modes require additional description for their anharmonicity (at least third order terms of $\boldsymbol{\xi}^{\rm SM}_{\mathbf{k},s}$), while the hard modes can be treated as harmonic oscillators (at least second order terms of $\boldsymbol{\xi}^{\rm HM}_{\mathbf{k},s}$). This leads to a picture that in the ordered phase the soft modes would presents finite displacements off their high symmetry positions while the hard modes are oscillating around their ones. It suggests $\left\langle \boldsymbol{\xi}^{SM} \right\rangle \gg \left\langle \boldsymbol{\xi}^{HM} \right\rangle$ in the issues of phase transitions, utilizing which

the hard modes terms could be treated as perturbations. Leaving out the high order terms, the potential energy of soft modes retaining the anharmonicity are expanded as

$$V_{\mathrm{SM}}^{(1)} = \sum_{\Omega^{\mathrm{SM}}} \left[ Q_{\mathbf{k},s}^{(2)} \left(\xi_{\mathbf{k},s}^{\mathrm{SM}}\right)^2 + Q_{\mathbf{k},s}^{(4)} \left(\xi_{\mathbf{k},s}^{\mathrm{SM}}\right)^4 \right] + \mathcal{O}\left(\left(\xi_{\mathbf{k},s}^{\mathrm{SM}}\right)^5\right), \tag{12}$$

$$V_{\mathrm{SM-HM}}^{(2)} = \sum_{\Omega^{\mathrm{SM}}} \sum_{\Omega^{\mathrm{HM}}} \left[ J_{\mathbf{k}\mathbf{k}',ss'}^{(1,1)} \xi_{\mathbf{k},s}^{\mathrm{HM}} \xi_{\mathbf{k}',s'}^{\mathrm{SM}} + J_{\mathbf{k}\mathbf{k}',ss'}^{(1,2)} \xi_{\mathbf{k}',s'}^{\mathrm{HM}} \left(\xi_{\mathbf{k},s}^{\mathrm{SM}}\right)^2 \right] + \mathcal{O}\left(\left(\xi_{\mathbf{k},s}^{\mathrm{SM}}\right)^3\right), \tag{13}$$

$$\begin{aligned} V_{\mathrm{SM-SM}}^{(2)} = \sum_{\Omega^{\mathrm{SM}}} \sum_{\Omega^{\mathrm{SM}}}{}' \Big[ & J_{\mathbf{k}\mathbf{k}',ss'}^{(1,1)} \xi_{\mathbf{k},s}^{\mathrm{SM}} \xi_{\mathbf{k}',s'}^{\mathrm{SM}} + J_{\mathbf{k}\mathbf{k}',ss'}^{(1,2)} \xi_{\mathbf{k},s}^{\mathrm{SM}} \left(\xi_{\mathbf{k}',s'}^{\mathrm{SM}}\right)^2 + J_{\mathbf{k}\mathbf{k}',ss'}^{(1,3)} \xi_{\mathbf{k},s}^{\mathrm{SM}} \left(\xi_{\mathbf{k}',s'}^{\mathrm{SM}}\right)^3 \\ & + J_{\mathbf{k}\mathbf{k}',ss'}^{(2,2)} \left(\xi_{\mathbf{k},s}^{\mathrm{SM}}\right)^2 \left(\xi_{\mathbf{k}',s'}^{\mathrm{SM}}\right)^2 \Big] + \mathcal{O}\left(\left(\xi_{\mathbf{k},s}^{\mathrm{SM}}\right)^3\right), \end{aligned} \tag{14}$$

where the prime in equation (14) requires either $\mathbf{k} \neq \mathbf{k}'$ or $s \neq s'$. $Q_{\mathbf{k},s}^{(n)}$ and $J_{\mathbf{k}\mathbf{k}'\cdots,ss'\cdots}^{(n,n',\cdots)}$ represents the interaction coefficients of one-body term and the many-body terms, where $n$ and $n'$ labels the orders of corresponding modes $\xi_{\mathbf{k},s}$. Here we also take the simplified notation requiring $n < n' < \cdots$ in $J_{\mathbf{k}\mathbf{k}'\cdots,ss'\cdots}^{(n,n',\cdots)}$ to avoid writing out the conjugate terms, e.g. $J_{\mathbf{k}\mathbf{k}',ss'}^{(1,2)} \xi_{\mathbf{k},s}^{\mathrm{SM}} \left(\xi_{\mathbf{k}',s'}^{\mathrm{SM}}\right)^2$ and $J_{\mathbf{k}\mathbf{k}',ss'}^{(2,1)} \left(\xi_{\mathbf{k},s}^{\mathrm{SM}}\right)^2 \xi_{\mathbf{k}',s'}^{\mathrm{SM}}$. The remained orders in one body terms are higher than many body terms, because the interaction magnitudes of the former are typically stronger than the latter ones. Only even order terms would enter the one-body part, which is due to the generally satisfied inverse symmetry in displacive FE materials, i.e. the polarizations can usually be switched between two equivalent states with opposite directions. In the same way, the potential energy of hard modes retaining harmonicity are expanded as

$$V_{\mathrm{HM}}^{(1)} = \sum_{\Omega^{\mathrm{HM}}} Q_{\mathbf{k},s}^{(2)} \left(\xi_{\mathbf{k},s}^{\mathrm{HM}}\right)^2 + \mathcal{O}\left(\left(\xi_{\mathbf{k},s}^{\mathrm{HM}}\right)^3\right), \tag{15}$$

$$V_{\mathrm{HM-HM}}^{(2)} = \sum_{\Omega^{\mathrm{HM}}} \sum_{\Omega^{\mathrm{HM}}}{}' J_{\mathbf{k}\mathbf{k}',ss'}^{(1,1)} \xi_{\mathbf{k},s}^{\mathrm{HM}} \xi_{\mathbf{k}',s'}^{\mathrm{HM}} + \mathcal{O}\left(\left(\xi_{\mathbf{k},s}^{\mathrm{HM}}\right)^2\right), \tag{16}$$

where the notations are the same as SM but are only kept up to second order terms.

A further simplification would be derived from the feature of the partition function that the contributions exponentially decay with $V_{\mathrm{n}}^{\mathrm{eff}}$ in equation (7). The SM with negative slope near the reference position corresponds to larger contributions to the effective potential than HM. It would be a good approximation to fix the HM related order terms to its ensemble average, as

$$\left[\xi_{\mathbf{k},s}^{\mathrm{HM}}\right]^i \rightarrow \left\langle \left[\xi_{\mathbf{k},s}^{\mathrm{HM}}\right]^i \right\rangle_T. \tag{17}$$

Applying harmonic approximation (HA) to HMs, we have the averages, as

$$\left\langle \xi_{\mathbf{k},s}^{\mathrm{HM}} \right\rangle_{\mathrm{HA}} = 0, \tag{18}$$

and the fluctuations, as

$$\left\langle \left[\xi_{\mathbf{k},s}^{\mathrm{HM}}\right]^2 \right\rangle_{\mathrm{HA}} = \frac{\hbar}{\omega_{\mathbf{k},s}} \left[ n_T(\hbar\omega_{\mathbf{k},s}) + \frac{1}{2} \right], \tag{19}$$

where $n_T(\hbar\omega_{\mathbf{k},s}) = \frac{1}{\mathrm{e}^{\beta\hbar\omega_{\mathbf{k},s}} - 1}$ is the number of the HMs at $T$. We could see it's reasonable to set $\left\langle \xi_{\mathbf{k},s}^{\mathrm{HM}} \right\rangle$ to zero and neglect the fluctuations at the HA level when $T$ is not too high. In so doing, $V_{\mathrm{HM}}^{(1)}$ and $V_{\mathrm{HM-HM}}^{(2)}$ enter the total effective Hamiltonian as constants, and the related SM–HM interaction would be emerged into $V_{\mathrm{SM}}^{(1)}$ and $V_{\mathrm{SM-SM}}^{(2)}$, the one body term of SM.

In total, we choose the magnitudes of soft phonon modes as the variables, and obtain the effective Hamiltonian in the form of

$$V_{\mathrm{n}}^{\mathrm{eff}} \approx V_{\mathrm{SM}}^{(1),\mathrm{eff}} + V_{\mathrm{SM-SM}}^{(2),\mathrm{eff}}, \tag{20}$$

where it should be noted that $V_{\mathrm{SM}}^{(1),\mathrm{eff}}$ and $V_{\mathrm{SM-SM}}^{(2),\mathrm{eff}}$ are slightly different from the ones in equations (12) and (14). The HM-SM interactions contribute as minor corrections to the intra- and interaction coefficients. This model could be systematically improved by including high order terms if needed. Accordingly, the partition function differs from the original one by constants

$$Z(\mathcal{H}_{\mathrm{tot}}) = A_{\mathrm{kin}} A_{\mathrm{e}} A_{\mathrm{HM}} Z(V_{\mathrm{n}}^{\mathrm{eff}}), \tag{21}$$

where $A_{\rm kin}$ represents the contribution of DOF of the momentum, and $A_{\rm e}$ and $A_{\rm HM}$ represents the contributions of electrons by Born–Oppenheimer approximation and common phonon modes by harmonic approximation, respectively.

As mentioned, $A$ relates close with the partition function of the integrated degrees of freedom. For simplicity, we consider a system consists of one soft mode $u$ and one hard mode $v$. In the case of this non-interacting system, we could divide the total energy into

$$E(u,v) = E_{\rm self}(u) + E_{\rm self}(v). \tag{22}$$

By definition, we obtain

$$A = \frac{Z^{\rm tot}}{Z^{\rm eff}} = \frac{\int {\rm d}p_u {\rm d}p_v {\rm d}u {\rm d}v {\rm e}^{-\beta E(u,v)}}{\int {\rm d}p_u {\rm d}u {\rm e}^{-\beta E_{\rm self}(u)}} = \int {\rm d}p_v {\rm d}v {\rm e}^{-\beta E_{\rm self}(v)}. \tag{23}$$

Here, $A$ is exactly the partition function of DOF of $v$. However, it's not such simple as if interaction between $u$ and $v$ is considered. In the interacting case, the total energy is

$$E(u,v) = E_{\rm self}(u) + E_{\rm self}(v) + E_{\rm int}(u,v). \tag{24}$$

Correspondingly, $A$ is now as

$$A = \frac{Z^{\rm tot}}{Z^{\rm eff}} = \frac{\int {\rm d}p_u {\rm d}u\ Z_v(u) {\rm e}^{-\beta E_{\rm self}(u)}}{\int {\rm d}p_u {\rm d}u\ {\rm e}^{-\beta E_{\rm eff}(u)}}, \tag{25}$$

$$Z_v(u) = \int {\rm d}p_v {\rm d}v {\rm e}^{-\beta [E_{\rm self}(v) + E_{\rm int}(u,v)]} \tag{26}$$

where $E_{\rm eff}(u)$ is the effective energy of $u$-DOF, and $Z_v(u)$ is the partition function of DOF of $v$ depends on $u$. As a hard mode, $v$ fluctuates around the equilibrium position. If the temperature is not too high, $v$ is closed to zero shown by equation (19) and we could approximate $E_{\rm eff}(u)$ to be $E_{\rm self}(u)$. Therefore, we would obtain

$$A \approx \frac{\int {\rm d}p_u {\rm d}u\ Z_v(u)\ {\rm e}^{-\beta E_{\rm self}(u)}}{\int {\rm d}p_u {\rm d}u\ {\rm e}^{-\beta E_{\rm self}(u)}} = \langle Z_v(u) \rangle_u \tag{27}$$

$A$ is the averaged partition function of v-DOF in this approximation.

### 2.2. Phonon related polarization

As mentioned, one would expect the description of FE properties from the constructed phonon related Hamiltonian. At high temperature, nuclei are averagely located at the high symmetry position and electrons distribute according to this configuration. No macroscopic polarizations are presented. When temperature becomes lower than the transition temperature, asymmetrical shifts of nuclei result in a permanent dipole moment. These atomic shifts can be described using collective patterns, which correspond to the FE soft modes. The total polarization is attributed to both the nuclear and electronic contributions, as

$$\Delta \mathbf{P} = \frac{e}{\Omega} \sum_I Z_n \Delta \mathbf{R}_I + \Delta \mathbf{P}_{\rm e}, \tag{28}$$

where $\Delta R_I$ is the displacement of the $I$th nuclei off its equilibrium position following the FE soft mode, and $eZ_n$ is the bare charge of the nuclei. Typically, the electronic part $\Delta \mathbf{P}_{\rm e}$ would seek a DFT solution. Modern polarization theory provides a rather simple picture. It indicates that for polarization the electron could also be treated as point charge localized at the centers of the Wannier function. The change in polarization can be expressed as

$$\Delta \mathbf{P}_{\rm e} = -\frac{e}{\Omega} \sum_i^{\rm occ} \left[ \langle 0i|\hat{\mathbf{r}}|0i\rangle^{\rm polarized} - \langle 0i|\hat{\mathbf{r}}|0i\rangle^{\rm unpolarized} \right], \tag{29}$$

where $|0i\rangle$ represents the ground state Wannier function [25, 26]. Resta *et al* have further shown that the displacement of the Wannier function center as well as the $\Delta P_{\rm e}$ is almost linear in the magnitude of FE modes [27]. This leads to an expression for the polarization with only FE mode, as

$$\mathbf{P} = \frac{e}{\Omega} \sum_I Z_I^\star \nu_I^{\rm FE} = \frac{e}{\Omega} Z_{\rm FE}^\star \boldsymbol{\xi}^{\rm FE}, \tag{30}$$

where the effective charges of one atom and FE mode is defined as

$$Z_I^\star := \frac{1}{e} \frac{{\rm d}\mathbf{P}}{{\rm d}\mathbf{R_I}} \text{ and } Z_{\rm FE}^\star := \frac{1}{e} \frac{{\rm d}\mathbf{P}}{{\rm d}\xi^{\rm FE}}. \tag{31}$$

$\nu_I^{\mathrm{FE}}$ is displacement pattern of the $I$th atom following the FE mode, $\xi^{\mathrm{FE}}$ is magnitude of the FE mode, and $Z_I^{\star}$ and $Z_{\mathrm{FE}}^{\star}$ are the Born effective charge of each atom and each FE mode, respectively. The mapping between FE mode and polarization also points out that the long-range interaction between FE modes is actually of the dipole–dipole interaction (DDI) form.

This also confirms that the effective Hamiltonian with soft phonon modes could describe both the ferroelectric and structural feature of displacive FE system. The usage of soft mode not only reduce the complexity of model but also capture the chief physical behaviors, making this method elegant and predictive.

### 2.3. Local mode approximation

The phonon modes variables are physically meaningful, however, not computationally expedient. Specifically, all phonon modes in subspace $\Omega^{\mathrm{SM}}$ should be considered. The corresponding interaction coefficients in equations (12) and (14) such as $Q_{\mathbf{k},s}^{(n)}$ and $J_{\mathbf{k}\mathbf{k}'\cdots,ss'\cdots}^{(n,n',\cdots)}$ depend on reciprocal vector $\mathbf{k}$ and are therefore complicated. Vanderbilt *et al* suggested the 'local mode approximation' that local modes could be used instead of the phonon modes, and the effective Hamiltonian is solved in real space [28]. These local modes are free from $\mathbf{k}$ dependencies and could be constructed from the phonon modes at high symmetry $\mathbf{k}$-points such as the Brillouin zone center and edge. The high symmetry $\mathbf{k}$-point means that the displacement patterns of the specified phonon mode in each own cell are the same, bringing the convenience that we could directly use the eigen vector of phonon modes. In so doing, the constructed modes are for sure localized in its own cell. It should be noted that the phonon mode represets for the collective motion of all lattice sites associated with $\mathbf{k}$-vector, while the local mode indicates the motion of its own site.

The local mode based representation is equivalent to the phonon mode based representation perceived from the same DOF. If we sample the phonon mode of $s$th branch in the reciprocal space, as

$$\left\{ \boldsymbol{\xi}_{\mathbf{k},s} \;\middle|\; \mathbf{k} = \sum_{n=1}^{3} \frac{l_n}{L_n}\mathbf{b}_n,\ l_n = 1, 2, \cdots, L_n \right\}, \tag{32}$$

where $\mathbf{b}_i$ is the basis vector of the reciprocal space, and $\frac{\mathbf{b}_n}{L_n}$ is the sampling spacing. The DOF of freedom are $L_1 \times L_2 \times L_3$ for one branch of phonon mode. For the corresponding local mode, e.g. the one constructed from the $\Gamma$ point, the same DOF could be obtained in real space, by

$$\left\{ u_{\mathbf{R}} \;\middle|\; \mathbf{R} = \sum_{n=1}^{3} l_n\mathbf{a}_n,\ l_n = 1, 2, \cdots, L_n \right\}, \tag{33}$$

where $\mathbf{a}_n$ is the basis vector of the real space. The aforementioned construction of local modes from phonon modes at high symmetry $\mathbf{k}$-points is a pratical way to derive approximated local basis. In principle, the local basis could be derived from the lattice Wannier functions (lattice WFs). Rabe *et al* gave the idea the local modes could be constructed employing the phonon informations of the whole Brillouin zone and interpreted that the local modes are actually the lattice analogue of electronic Wannier functions [29, 30]. This lattice WFs are not unique. Like the searching for the maximum localized Wannier function (MLWF) of electrons, here we also expect MLWF of the lattice. This is because that a more localized basis set would bring less intersite overlaps, and consequently a simpler many-body interaction which decays rapidly in the real space. In the cases that soft modes are not mainly associated with high symmetry $\mathbf{k}$-points, one could only resort to the lattice WFs. However, there might be some difficulties in generally deriving the best lattice WFs (the best means one might expect the lattice WF localized in one own site), parameterization process, and interpretation of the physical meaning of the coefficients. For displacive FE materials, where typically ferroelectricity associates with high symmetry $\mathbf{k}$-points, we would adopt the aforementioned constructed local mode and check the mode pattern with experimental observations. For example, the local modes for the $ABO_3$ perovskite compounds are usually choose to be (1) FE modes at $\Gamma$ point, presenting as the relative motion of A, B, and O; (2) AFD modes at $M$ or $R$ point, presenting as the rotation of the octahedron of O atom. Both of these modes can not only be observed in experiments but also derived from first-principles phonon calculations. This coincidence also confirms the validity of local mode approximation.

Applying the local mode approximation, the effective Hamiltonian is now written as

$$V_{\mathrm{n}}^{\mathrm{eff}} = \sum_{u} V_{\mathrm{n}}^{(1)}(u) + \sum_{u}\sum_{v} V_{\mathrm{n}}^{(2)}(u, v), \tag{34}$$

with the one-body terms

$$V_{\mathrm{n}}^{(1)}(u) = \sum_{\mathbf{R}} \left[ Q_u^{(2)} \left(u_{\mathbf{R}}\right)^2 + Q_u^{(4)} \left(u_{\mathbf{R}}\right)^4 \right] + \mathcal{O}\left(\left(u_{\mathbf{R}}\right)^5\right), \tag{35}$$

and two-body terms

$$V_{\mathrm{n}}^{(2)}(u,v)=\sum_{\mathbf{R}}\sum_{\mathbf{R}'}{}'\left[J_{\Delta\mathbf{R},uv}^{(1,1)}u_{\mathbf{R}}v_{\mathbf{R}'}+J_{\Delta\mathbf{R},uv}^{(1,2)}u_{\mathbf{R}}\left(v_{\mathbf{R}'}\right)^{2}+J_{\Delta\mathbf{R},uv}^{(1,3)}u_{\mathbf{R}}\left(v_{\mathbf{R}'}\right)^{3}+J_{\Delta\mathbf{R},uv}^{(2,2)}\left(u_{\mathbf{R}}\right)^{2}\left(v_{\mathbf{R}'}\right)^{2}\right]+\mathcal{O}\left(u_{\mathbf{R}}^{3}\right),\tag{36}$$

where $u_{\mathbf{R}}$ and $v_{\mathbf{R}}$ are the magnitudes of the local modes localized at $\mathbf{R}$ site, and $\Delta\mathbf{R}=\mathbf{R}-\mathbf{R}'$ is the distance between the two sites. The sites are identical, hence that $Q_u^{(2)}$ and $Q_u^{(4)}$ are independent of $\mathbf{R}$. And further, the two body interaction coefficients $J_{\mathbf{R}\mathbf{R}',uv}^{(n,n')}$ turns to be $J_{\Delta\mathbf{R},uv}^{(n,n')}$.

Now we could also obtain the dipole moment of each site by FE local modes

$$\mu_{\mathbf{R}}=\frac{e}{\Omega_{\mathrm{cell}}}Z^{\star}u_{\mathbf{R}}^{\mathrm{FE}}\mathbf{e}_u,\tag{37}$$

where the orientation of polarization is determined by the unit vector $\mathbf{e}_u$ of mode pattern. Since the long-range part of the two body interaction is mainly DDI of FE modes, we can further decompose equation (36) into

$$V_{\mathrm{n}}^{(2)}=V_{\mathrm{n,short}}^{(2)}+V_{\mathrm{n,long}}^{(2)},\tag{38}$$

with the short-range part

$$V_{\mathrm{n,short}}^{(2)}=\sum\sum_{|\Delta\mathbf{R}|<R_{\mathrm{cut}}}\left[K_{\Delta\mathbf{R},uv}^{(1,1)}u_{\mathbf{R}}v_{\mathbf{R}'}+J_{\Delta\mathbf{R},uv}^{(1,2)}u_{\mathbf{R}}\left(v_{\mathbf{R}'}\right)^{2}+J_{\Delta\mathbf{R},uv}^{(1,3)}u_{\mathbf{R}}\left(v_{\mathbf{R}'}\right)^{3}+J_{\Delta\mathbf{R}}^{(2,2)}\left(u_{\mathbf{R}}\right)^{2}\left(v_{\mathbf{R}'}\right)^{2}\right],\tag{39}$$

and the long-range part

$$V_{\mathrm{n,long}}^{(2)}=\sum\sum_{\mathrm{FE}}\frac{\mu_{\mathbf{R}}\cdot\mu_{\mathbf{R}'}-3\left(\mu_{\mathbf{R}}\cdot\Delta\mathbf{R}\right)\left(\mu_{\mathbf{R}'}\cdot\Delta\mathbf{R}\right)}{\epsilon\left(\Delta\mathbf{R}\right)^{3}}.\tag{40}$$

Here $K_{\Delta\mathbf{R},uv}^{(1,1)}$ is the remaining part of $J_{\Delta\mathbf{R},uv}^{(1,1)}$ excluding DDI. The first summation is truncated to $R_{\mathrm{cut}}$ in real space for all soft modes, and the second summation is DDI which is only valid for FE modes. The DDI could be solved by regular numerical method such as the Ewald summation. For FE modes, the first term tracked the deviation between the interacting picture of modeling them as point dipoles and the real one. All the other short-range interactions, such as the short-range repulsion and electronic hybridization between neighboring local modes, are expected to enter the first term. For the other modes, the short-range interaction have the same origin as FE modes. But there's no evidence that they own significant long range interactions. Indeed, the atoms are relatively heavy and localized hence to little long range correlation. We would consider the interactions only for the modes which share atoms. For example, it is typically up to 3rd nearest neighbor (NN) sites for cubic structure, since 1st/2nd/3rd NN sites share the atoms of a plane/edge/corner. For convenience, we would call the first term as short-range interaction (with short-range part of DDI excluded) and the second term as long-range interaction without distinguishing FE modes and the other modes. Comparing to equations (12) and (14), the interaction coefficients in equations (35), (39) and (40) have been greatly simplified. We could obtain these coefficients through limited first-principles calculations.

### 2.4. *NpT* ensemble

The aforementioned construction of effective Hamiltonian is based on the *NVT* ensemble. With the softening of soft modes, however, the displacive FE material presents structural phase transition simultaneously. For instance, $SrTiO_3$ undergoes a transition from cubic structure to tetragonal with the softening of the AFD modes, and SnTe undergoes a transition from cubic to rhombohedral with the softening of the FE modes. This would require us using *NpT* ensemble instead of *NVT* ensemble and counting in the elastic energy contribution.

The partition function for *NpT* ensemble is written as

$$Z_{NpT}(\mathcal{H}^{\mathrm{ori}})=\int\mathrm{d}\Omega\int\mathrm{d}^{3N}p_i\int\mathrm{d}^{3N}r_i\exp\left[-\beta(\mathcal{H}^{\mathrm{ori}}(p_i,r_i)+p_{\mathrm{ext}}\Omega)\right],\tag{41}$$

where $p_{\mathrm{ext}}$ is the external pressure. The varied volume explicitly influence the $p_{\mathrm{ext}}\Omega$ term. In fact, the elastic energy and the coupling energy with local modes should also be concerned. The elastic energy describe the consumed energy when driving the system off the equilibrium volume. The long-range interaction of local modes, DDI depends on the distances between dipoles. The short-range part, which arise from the shared atoms and electrons between neighboring sites, is also affected by the distance between sites. Thus, the volume related potential energy has three parts, as

$$V_{\Delta\Omega}=V_{\mathrm{elastic}}+V_{\mathrm{pc}}+V_{\mathrm{lmc}},\tag{42}$$

where the three terms correspond to the elastic, pressure coupling, and local mode coupling contributions, respectively. Introducing the Voigt notation, we express the strain tensor of each site as

$$\eta_{\mathbf{R}l} = \eta_l^{\mathrm{H}} + \eta_{\mathbf{R}l}^{\mathrm{IH}}, \tag{43}$$

where the homogeneous part $\{\eta_l^{\mathrm{H}}\}$ and the inhomogeneous part $\{\eta_{\mathbf{R}l}^{\mathrm{IH}}\}$ are introduced. Here the $l = 1, 2, 3$ components present the diagonal part of the strain tensor (lattice contraction and expansion), and $l = 4, 5, 6$ components present the shear part. $\eta_l^{\mathrm{H}}$ and $\eta_{\mathbf{R}l}^{\mathrm{IH}}$ characterize the macroscopic deformation of the material and microscopic deformation of each cell in addition to the homogeneous part, respectively. The $\eta_{\mathbf{R}l}^{\mathrm{IH}}$ is essential in describing the domain structure or material consists of local structure such as layer-stacking perovskites. When focusing on macroscopic properties such as the phase transition, $\eta_{\mathbf{R}l}^{\mathrm{IH}}$ shows fluctuation behaviors upon equilibrium and could be set to zero for convenience. Formally, we expand the volume related energy contributions as a power series in strain tensors around the volume of reference structure, as

$$V_{\mathrm{elastic}} = \frac{1}{2}\sum_{\mathbf{R}l} C_{ll}(\eta_{\mathbf{R}l})^2 + \sum_{\mathbf{R}l}\sum_{\mathbf{R}m} C_{lm}\eta_{\mathbf{R}l}\eta_{\mathbf{R}m} + \sum_{\mathbf{R}l}\sum_{\mathbf{R}'m} A_{il,jm}\eta_{\mathbf{R}l}^{\mathrm{IH}}\eta_{\mathbf{R}'m}^{\mathrm{IH}}, \tag{44}$$

where $C_{lm}$ is the elastic constant matrix, $A_{il,jm}$ characterizes the elastic interaction between neighboring cell $i$ and $j$ induced by inhomogeneity. And the other two terms are

$$V_{\mathrm{pc}} = p_{\mathrm{ext}} \cdot \Delta\Omega = p_{\mathrm{ext}}\Omega(\eta_1^{\mathrm{H}} + \eta_2^{\mathrm{H}} + \eta_3^{\mathrm{H}}), \tag{45}$$

$$V_{\mathrm{lmc}} = \frac{1}{2}\sum_{\mathbf{R}l}\sum_{u}\sum_{v} B_{luv}\eta_{\mathbf{R}l}u_{\mathbf{R}}v_{\mathbf{R}}, \tag{46}$$

where $u$ and $v$ are for local modes (could be the same mode) at the $\mathbf{R}$ site. In equation (46), the nonlocal coupling between strain at $\mathbf{R}$ site and local mode at $\mathbf{R}' \neq \mathbf{R}$ site is ignored, and only leading terms of the local coupling are remained in associate with former expansion on local modes. It should be noted that by frozen $\eta_{\mathbf{R}l}$, the coupling terms in equation (46) actually contribute as corrections to coefficients of the two-body interactions between local modes. To avoid double counting, we should perform the evaluation of equation (40) at the reference structure instead of the instantaneous structure in the simulation.

Combining equations (35), (39), (40) and (44)–(46), we obtain the effective Hamiltonian for $NpT$ ensemble, as

$$V_{NpT}^{\mathrm{eff}} = V_{\mathrm{n}}^{(1)} + V_{\mathrm{n,short}}^{(2)} + V_{\mathrm{n,long}}^{(2)} + V_{\mathrm{elastic}} + V_{\mathrm{pc}} + V_{\mathrm{lmc}}. \tag{47}$$

Upon the construction, this Hamiltonian is expected to describe both ferroelectric and structural properties. The remaining task is the parameterization of the coefficients by DFT calculations and simulation performed with this effective Hamiltonian.

## 3. Implementation and examples

In this section, we describe the practical procedure for the implementation of the effective Hamiltonian. We give a general scheme at first and then show material-specific treatment for 3D and 2D SnTe. A potential use for a rather complicated system, i.e. M-type hexaferrites, is discussed later.

### 3.1. General procedure

In general, the implementation for one specific displacive FE material would have following steps:

1. Choose the high symmetry structure of the material as the reference, and calculate the corresponding phonon spectrum via DFT. Typically the most stable structure at high $T$ could meet the requirements. Besides, linear response calculations to derive the dielectric constant and Born effective charge should also be performed.
2. Determine the local modes and the subspace using the eigen vector of several phonon modes at high symmetry $k$-points. If the phonon spectrum is largely deviate from experiments and even indicates none soft mode, check and improve the accuracy by using a higher level DFT functional. For instance, it was reported that LDA and PBE functional cannot reproduce the softening of FE mode in SnTe, while SCAN functional performs well.
3. Construct several configurations in the subspace where the atoms are displaced by the pattern of local modes and calculate their energy. These configurations can be generated by giving random magnitudes of local modes at each site. Since there're finite coefficients of 2–4 orders of magnitude, an efficient way is to construct configurations upon high symmetry $k$-points.

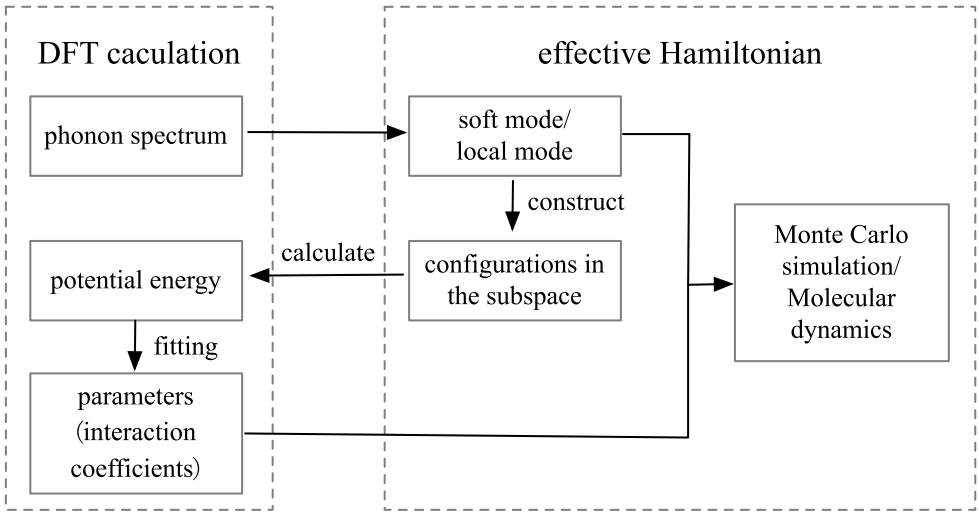


**Figure 1.** The flowchart of implementation. DFT calculations are required to determine the local modes and interaction coefficients. Subsequently, the effective Hamiltonian is simulated with Monte Carlo or molecular dynamics.

4. Fitting the coefficients from the sampled energy profile. Check the relationship among coefficients. For example, the coefficients of short-range interaction should decay rapidly, if not, high order terms or other type of long-range interaction besides DDI should be considered. The expansion in former section is up to fourth order of soft modes to include at least anharmonicity, and could be extended to sixth order in a similar way if necessary.
5. Using the DFT derived parameters, perform simulations with either Monte Carlo method or molecular dynamics depending on research interests. The results can provide the finite $T$ statistics on the magnitudes of local modes, i.e. a series of instantaneous atomic configurations. The phonon related or structure related estimators are resorted to evaluate properties of interests.

A general implementation procedure is sketched in figure 1.

### 3.2. Rocksalt type group-IV monochalcogenides

Rocksalt type group-IV monochalcogenides exhibit cubic symmetry (in its Bravais cell) at high $T$. The Bravais cell instead of the primitive cell are used, because the former one provides a simpler interaction form than the oblique cells. SnTe material is taken here as an example. It was reported that the SnTe thin films exhibit robust inplane ferroelectricity [31]. This phenomenon is interesting for the unusual thickness dependency, which violates the finite size scaling law and enables potential ultrathin devices. We used the aforementioned effective Hamiltonian to study this material. Here, we focus on the construction of the effective Hamiltonian of SnTe in 3D and 2D cases. Besides, two practical problems are tackled: (1) the Monte Carlo simulation procedure; (2) the pressure compensation used to correct the simulated results. The corresponding simulation results have been reported in our published paper [32].

#### *3.2.1. Hamiltonian for 3D case*

The 8 atoms of SnTe's Bravais cell (consist of 4 Sn atoms and 4 Te atoms) allow 24 branches of phonon modes, and DFT calculations with SCAN functional confirm at $\Gamma$ the three of 21 optical modes are the softest modes. Correspondingly, we construct three local modes for SnTe to be the relative motion between Sn and Te atom labeled as $u_1$, $u_2$, and $u_3$. Due to the three-fold degeneracy of the soft modes and each of the three modes is along one axis of $x, y, z$, we relabel them as a vector

$$\mathbf{u} = (u_1, u_2, u_3) = \left(u_x, u_y, u_z\right). \tag{48}$$

The interaction coefficients such as $J^{(n,n')}_{\Delta\mathbf{R},uv}$ are replaced with $J^{(n,n')}_{\Delta\mathbf{R},\alpha\beta}$ accordingly. Besides, we leave out the inhomogeneous strain $\eta^{\mathrm{IH}}_{\mathbf{R}l}$ since the interested para-ferroelectric phase transition is mainly concerned with uniformed deformation throughout the lattice. Thus, the variables for SnTe are $\left\{\mathbf{u}_{\mathbf{R}}, \eta^{\mathrm{H}}_{l}\right\}$, and we will use the cubic symmetry to simplify the interaction coefficients.

We follow the expansion in previous section to fourth order of $\mathbf{u}_{\mathbf{R}}$ and to second order of $\eta^{\mathrm{H}}_{l}$. In total, the effective Hamiltonian requires the following coefficients:

$$Q_{\alpha}^{(2)},\ Q_{\alpha}^{(4)},\ K_{\Delta\mathbf{R},\alpha\beta}^{(1,1)},\ J_{\Delta\mathbf{R},\alpha\beta}^{(1,2)},\ J_{\Delta\mathbf{R},\alpha\beta}^{(1,3)},\ J_{\Delta\mathbf{R},\alpha\beta}^{(2,2)},\ C_{ll},\ B_{l\alpha\beta}, \tag{49}$$

where the notations is the same as in equations (35), (39), (40) and (44)–(46), except for replacement of the local mode labels from $u/v$ to $\alpha/\beta = x, y, z$ according to equation (48). Because of the rotation symmetry of the three modes, the one-body coefficients turn to be

$$Q_{\alpha}^{(2)} = Q_{\beta}^{(2)} = Q^{(2)},\ \text{and}\ Q_{\alpha}^{(4)} = Q_{\beta}^{(4)} = Q^{(4)}. \tag{50}$$

We set the cutoff for the lowest order short-range interaction $K_{\Delta\mathbf{R},\alpha\beta}^{(1,1)}$ to third nearest neighbor (NN) site, and the other higher order term including $J_{\Delta\mathbf{R},\alpha\beta}^{(1,2)}, J_{\Delta\mathbf{R},\alpha\beta}^{(1,3)}, J_{\Delta\mathbf{R},\alpha\beta}^{(2,2)}$ to local site. The notation $J_{\Delta\mathbf{R},uv}^{(n,n')}$ naturally satisfies the intersite permutation and periodicity. Further utilizing the crystal symmetry, we would obtain several nonzero and unique coefficients. Generally if a symmetry operation $O$ can map the local mode $u_{\alpha}$ to $u'_{\beta} = O(u_{\alpha})$, the coefficients $J_{\mathbf{RR}'\cdots,\alpha\beta\cdots}$ should satisfies

$$\sum_{\alpha\beta\cdots} J_{\mathbf{RR}'\cdots,\alpha\beta\cdots} O_{\alpha\alpha'} O_{\beta\beta'} \cdots = J_{O(\mathbf{R})O(\mathbf{R}')\cdots,\alpha'\beta'\cdots}. \tag{51}$$

It should be noted that the $n$-order terms should be treated $n$ times, e.g. $J_{\mathbf{RR}',\alpha\beta}^{(1,2)}$ should be treated as $J_{\mathbf{RR}'\mathbf{R}',\alpha\beta\beta}$ here. Especially for two body interactions

$$\sum_{\alpha\beta} J_{\Delta\mathbf{R},\alpha\beta} O_{\alpha\alpha'} O_{\beta\beta'} = \sum_{\alpha\beta} J_{\mathbf{RR}',\alpha\beta} O_{\alpha\alpha'} O_{\beta\beta'} = J_{O(\mathbf{R})O(\mathbf{R}'),\alpha'\beta'} = J_{O(\Delta\mathbf{R}),\alpha'\beta'}, \tag{52}$$

where the last equality utilizes $O(\Delta\mathbf{R}) = O(\mathbf{R}) - O(\mathbf{R}')$. For example, $K_{\mathbf{a}_x,xy}^{(1,1)}$ is always zero because of the equality

$$K_{\mathbf{a}_x,xy}^{(1,1)} = -K_{-\mathbf{a}_x,xy}^{(1,1)} = -K_{\mathbf{a}_x,xy}^{(1,1)}. \tag{53}$$

The first equality is derived with $x$-inverse symmetry operator

$$O_{x\to -x} = \begin{bmatrix} -1 & 0 & 0 \\ 0 & 1 & 0 \\ 0 & 0 & 1 \end{bmatrix} \tag{54}$$

and the second one is derived with $x, y$-inverse symmetry operator

$$O_{x\to -x, y\to -y} = \begin{bmatrix} -1 & 0 & 0 \\ 0 & -1 & 0 \\ 0 & 0 & 1 \end{bmatrix}. \tag{55}$$

The equality $K_{\mathbf{a}_x,xy}^{(1,1)} = -K_{\mathbf{a}_x,xy}^{(1,1)}$ leads to $K_{\mathbf{a}_x,xy}^{(1,1)} = 0$. For the two body interactions between local modes, the unique terms are

$$\text{1st NN}:\ K_{\mathbf{a}_x,xx}^{(1,1)}, K_{\mathbf{a}_x,yy}^{(1,1)}, \tag{56}$$

$$\text{2nd NN}:\ K_{\mathbf{a}_{x+y},xx}^{(1,1)}, K_{\mathbf{a}_{x+y},xy}^{(1,1)}, K_{\mathbf{a}_{x+y},zz}^{(1,1)}, \tag{57}$$

$$\text{3rd NN}:\ K_{\mathbf{a}_{x+y+z},xx}^{(1,1)}, K_{\mathbf{a}_{x+y+z},xy}^{(1,1)}, \tag{58}$$

$$\text{local site}:\ J_{0,xy}^{(2,2)}, \tag{59}$$

where $\mathbf{a}_{x,y,z}$ are the lattice basis. And the unique elements of the elastic constant matrix are

$$C_{11},\ C_{12},\ C_{44}, \tag{60}$$

and the unique coupling coefficients between local modes and strains are

$$B_{1xx},\ B_{1yy},\ B_{4yz}. \tag{61}$$

The first-principles calculations are implemented to fit these unique coefficients as done in [32], and these parameters are given in table 1.

As mentioned, we have supposed that the long-range interaction is almost of DDI type and the rest is of short-range feature. This postulation can be checked here by watching the tendency of short-range interaction magnitude towards farther sites. If the magnitude of so-called short-range interaction does not decay fast in real space, it means other type of long-range interaction should be considered. This procedure also gives the cutoff for $K_{\Delta\mathbf{R},\alpha\beta}^{(1,1)}$ and $J_{\Delta\mathbf{R},\alpha\beta}^{(2,2)}$. The ratio of strongest interaction coefficients of 1st NN, 2nd NN, and 3rd NN comes to be 1 : 0.180 : 0.014. Considering that there are 6 FNNs, 12 SNNs, and 8 TNNs, the ratio of energy contributions comes

**Table 1.** Parameters of the effective Hamiltonian for SnTe. Energies are in hartrees. The notation is the same as in equation (35), (39), (40) and (44)–(46). For convenience, original notations in [16] and [32] are given in the brackets.

| | | | | | | | |
|---|---|---|---|---|---|---|---|
| $V_{\mathrm{n}}^{(1)}$ | | $Q_{\alpha}^{(2)}(\kappa_2)$ | 0.0128 | $Q_{\alpha}^{(4)}(\alpha_4)$ | 0.0140 | | |
| $V_{\mathrm{n,long}}^{(2)}$ | | $\epsilon$ | 51.9 | $Z_{\mathrm{FE}}^{*}$ | 19.9 | | |
| $V_{\mathrm{n,short}}^{(2)}$ | local | $J_{0,xy}^{(2,2)}(\gamma_4)$ | −0.009 71 | | | | |
| | 1st NN | $K_{\mathbf{a}_x,yy}^{(1,1)}(j_1)$ | −0.004 07 | $K_{\mathbf{a}_x,xx}^{(1,1)}(j_2)$ | 0.000 402 | | |
| | 2nd NN | $K_{\mathbf{a}_{x+y},xx}^{(1,1)}(j_3)$ | 0.000 128 | $K_{\mathbf{a}_{x+y},zz}^{(1,1)}(j_4)$ | −0.000 731 | $K_{\mathbf{a}_{x+y},xy}^{(1,1)}(j_5)$ | 0.000 457 |
| | 3rd NN | $K_{\mathbf{a}_{x+y+z},xx}^{(1,1)}(j_6)$ | 0.000 0582 | $K_{\mathbf{a}_{x+y+z},xy}^{(1,1)}(j_7)$ | 0.000 0291 | | |
| $V_{\mathrm{elastic}}$ | | $C_{11}$ | 6.82 | $C_{12}$ | 0.0972 | $C_{44}$ | 1.09 |
| $V_{\mathrm{lmc}}$ | | $B_{1xx}$ | −0.264 | $B_{1yy}$ | −0.0270 | $B_{4yz}$ | −0.0165 |
| 2D corr | | $A_{\mathbf{a}_x,xx}^{(1,1)}$ | −0.007 22 | $1/n_c$ | −0.376 | | |

to be 1 : 0.360 : 0.018. Due to this fast decay behavior, the ignored parts would bring slight contributions. It also means that our postulation is reasonable and the cutoff up to TNN is enough.

Here, we have derive all the energy terms in analytical and practical expressions except for $V_{\mathrm{n,long}}^{(2)}$. The long-range interaction of DDI type in equation (40) is treated following the regular Ewald summation method for 3D case (EW3D) [33]. We write the DDI into three parts, as

$$V_{\mathrm{n,long}}^{(2)} = V_{\mathrm{rspace}} + V_{\mathrm{kspace}} + V_{\mathrm{corr}}, \tag{62}$$

where the three terms are real space term, kspace term, and the correction term, respectively.

$$V_{\mathrm{rspace}} = \frac{1}{2}\sum_{\mathbf{R}\mathbf{R}'}\sum_{|\mathbf{a}_n|=0}^{\infty}{}' \Big[(\mu_{\mathbf{R}}\cdot\mu_{\mathbf{R}'})B(\Delta\mathbf{R}+\mathbf{a}_n) - (\mu_{\mathbf{R}}\cdot\Delta\mathbf{R})(\mu_{\mathbf{R}'}\cdot\Delta\mathbf{R})C(\Delta\mathbf{R}+\mathbf{a}_n)\Big], \tag{63}$$

with

$$B(r) = \frac{\mathrm{erfc}(\kappa r)}{r^3} + \frac{2\kappa}{\sqrt{\pi}}\frac{\mathrm{e}^{-\kappa^2 r^2}}{r^2}, \tag{64}$$

$$C(r) = \frac{3\mathrm{erfc}(\kappa r)}{r^5} + \frac{2\kappa}{\sqrt{\pi}}\frac{(2\kappa^2 r^2+3)}{r^2}\frac{\mathrm{e}^{-\kappa^2 r^2}}{r^2}, \tag{65}$$

where $\kappa$ is the Ewald parameter, and $\mu_{\mathbf{R}}$ is the dipole at site $i$, and $\mathbf{a}_n$ represents the lattice vector $\{n_x\mathbf{a}_x + n_y\mathbf{a}_y + n_z\mathbf{a}_z | n_{x,y,z} \in Z\}$. $V_{\mathrm{rspace}}$ sums over all pair $\langle\mathbf{R},\mathbf{R}'\rangle$ and all integer vector $\mathbf{a}_n$, with the prime meaning excluding $i=j$ for $|\mathbf{a}_n|=0$. And the k-space term can quickly converge in kspace

$$V_{\mathrm{kspace}} = \frac{1}{2}\sum_{\mathbf{R}\mathbf{R}'}\sum_{\mathbf{k}\neq 0}\frac{4\pi}{k^2L^3}(\mu_{\mathbf{R}}\cdot\mathbf{k})(\mu_{\mathbf{R}'}\cdot\mathbf{k})\mathrm{e}^{-\frac{k^2}{4\kappa^2}}\cos(\mathbf{k}\cdot\Delta\mathbf{R}), \tag{66}$$

where $\mathbf{k}$ labels the reciprocal lattice vector. And the correction term is

$$E_{\mathrm{corr}} = -\sum_{\mathbf{R}}\frac{2\kappa^3}{3\sqrt{\pi}}\mu_{\mathbf{R}}^2 + \frac{1}{2}\sum_{\mathbf{R}\mathbf{R}'}\frac{4\pi}{3L^3}\mu_{\mathbf{R}}\cdot\mu_{\mathbf{R}'}. \tag{67}$$

One finite-$T$ FE modes configuration on strained lattice is shown schematically in figure 2. We set a finite temperature $T$ and external pressure $p_{\mathrm{ext}}$, allowing FE modes $\{\mathbf{u}_i,\ i=1,2,\cdots,N\}$, lattice strain $\{\eta_l,\ l=1,2,\cdots,6\}$ varied to achieve thermal equilibrium. Then we do statics on $u_{x,y,z} = \langle u_i\rangle_{x,y,z}$ and $\{\eta_l,\ l=1,2,\cdots,6\}$ to tell the properties of the system at finite-$T$. The structural information is given by the distorted lattice and displaced atomic positions. Ferroelectric properties are described by the alignments of FE modes. When they are aligned uniformly to one direction, a FE phase is determined and the magnitude of polarization is given by equation (37). And when they are aligned randomly with the statistical average to be zero, a PE phase is determined.

### 3.2.2. *Hamiltonian for 2D case*

Coming to the 2D case, the effective Hamiltonian must be modified to restore the varied electronic structure. Generally, there're two equivalent approaches to this goal: (1) restart from a 2D reference structure and its corresponding 2D local modes, construct a new effective Hamiltonian; (2) based on the 3D effective Hamiltonian and bulk local modes, introduce corrections to film interactions. Here we adopt the latter for three reasons. At

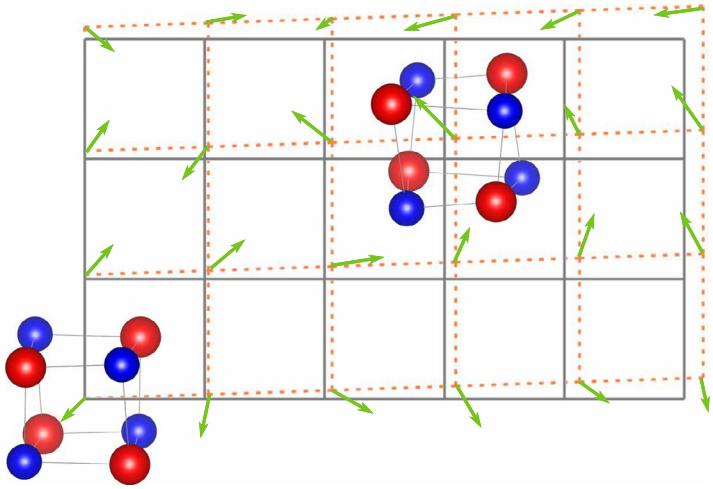

**Figure 2.** A schematic of the effective potential. The reference structure (grey solid lines) is distorted by lattice strain $\eta$ (orange dashed lines) and FE modes $\mathbf{u}_i$ i.e. the polarization (green arrows). Their intra- and interactions are used later to perform the Monte-Carlo simulations.

first, the latter can build the bridge between bulk and thin films, upon which understand the abnormal behavior of $T_c$ in SnTe [31]. By using bulk soft mode, it is clear that changes from bulk to films originate from geometry changes (mainly in long-range dipole–dipole interaction) and electronic changes (mainly in the short-range interactions). Secondly, the latter is methodologically simple and computationally practical to studies the film behavior for a series of number of layers. The former requires resampling the whole energy profile for each number of layers and subsequent heavy DFT calculations, while the latter requires resampling several configurations. At last, extrinsic strain effects can be treated only by using a same reference structure. An extra pressure is used to compensate insufficiently accurate electronic structure. If different reference structure are used, the error of compensation pressure might mislead the results. A detailed discussion about pressure compensation is given in next subsection.

The fundamental difference between the bulk and film is the presence of surface. From bulk to thin film, the periodicity is broken at the surface. The electrons, which should distribute near the boundary in bulk, spread to inner zone in thin film. This means more correlations originated from electrons and hence to the correction of original interaction of nuclei. According to this, we check each energy term of the 3D effective Hamiltonian if correction is needed. The one-body terms $V_{\mathrm{n}}^{(1)}$ comes from the isolated on-site energy of the local modes. If the reference structure and local mode remain unchanged, $V_{\mathrm{n}}^{(1)}$ should remain unchanged no matter when its surrounding sites form a 2D geometry or a 3D geometry. $V_{\mathrm{n,long}}^{(2)}$ would receive changes upon going to films, however, mainly from the geometry changes (lattice contraction in out-of-plane direction and expansion in in-plane direction). The picture of point dipoles at each site from macroscopic viewing remains unchanged. By definition, the short-range terms $V_{\mathrm{n,short}}^{(2)}$ are mostly affected. Therefore, we consider only geometry changes in dipole–dipole interaction terms as $V_{\mathrm{n,long,2D}}^{(2)}$, and count all the other surface effects in short range terms (add corrections to $V_{\mathrm{n,short}}^{(2)}$ as $V_{\mathrm{corr,2D}}^{(2)}$). The total of the energy in 2D geometry is written as:

$$V_{\mathrm{2D}}^{\mathrm{eff}} = V_{\mathrm{n}}^{(1)} + V_{\mathrm{n,short}}^{(2)} + V_{\mathrm{corr,2D}}^{(2)} + V_{\mathrm{n,long,2D}}^{(2)} + V_{\mathrm{elastic}} + V_{\mathrm{pc}} + V_{\mathrm{lmc}} \tag{68}$$

where only $V_{\mathrm{corr,2D}}^{(2)}$ and $V_{\mathrm{n,long,2D}}^{(2)}$ are different from the 3D case. $V_{\mathrm{corr.2D}}^{(2)}$ depends on the number of layers. Indeed, it should meet the prerequisite that the correction terms $V_{\mathrm{corr,2D}}^{(2)}$ vanish spontaneously upon reaching the bulk (by increasing the film thickness to infinity). Considering that the 2D features is gradually lost and with a weaker tendency in this procedure, we characterize the changed interactions by the form of exponential decay in thickness (or equivalently the number of layers). We take the form of [34] and add the exponential decay coefficients to describe this layer dependency, as

$$V_{\mathrm{corr,2D}}^{(2)}(n_l) = \sum_{\alpha=\beta} \sum_{\Delta\mathbf{R}=\mathbf{a}_\alpha} \mathrm{e}^{-n_l/n_c} A_{\Delta\mathbf{R},\alpha\beta}^{(1,1)} u_{\mathbf{R}\alpha} u_{\mathbf{R}'\beta}, \tag{69}$$

where $n_l$ labels the number of layers and $n_c$ is the character number of layers, $A_{\Delta\mathbf{R},\alpha\beta}^{(1,1)}$ is the coefficients of the short range corrections (exclude the short part correction of dipole–dipole interactions) between $\mathbf{R}$ and $\mathbf{R}'$ sites. Here we have constrained the correction only to intersite pairs $u_{\mathbf{R}\alpha}$ and $u_{\mathbf{R}'\beta}$ for $\Delta\mathbf{R} = \mathbf{a}_\alpha$ and $\alpha = \beta = x, y$. The correction can be regarded as perturbation to the original 3D Hamiltonian, we take only its leading term.

As mentioned, the short range interaction is basically from sharing atoms. The above intersite pairs maximally shares atom (the modes are head-to-head and shares a plane), than the other pairs.

In practical, Ewald summation for 2D case (EW2D) [35] instead of EW3D [33] should be used to solve the $V^{(2)}_{\mathrm{n,long,2D}}$ terms in the Hamiltonian due to the film geometry. In the same as EW3D in equation (62), EW2D also writes the DDI in three parts

$$V^{(2)}_{\mathrm{n,long,2D}} = V_{\mathrm{rspace}} + V_{\mathrm{kspace,2D}} + V_{\mathrm{corr,2D}}, \tag{70}$$

where the real space term is the same as bulk, but kspace terms $V_{\mathrm{kspace,2D}}$ and correction terms $V_{\mathrm{corr,2D}}$ are different, as

$$\begin{aligned} E_{\mathrm{k}} =& \frac{1}{2}\sum_{\mathbf{RR}'}\sum_{\mathbf{k}\neq 0}\frac{\pi}{L^2}\mathrm{e}^{\mathrm{i}\mathbf{k}\cdot\rho_{\Delta\mathbf{R}}}\Big\{(\mu^{\rho}_{\mathbf{R}}\cdot\mathbf{k})(\mu^{\rho}_{\mathbf{R}'}\cdot\mathbf{k})D(z_{ss'}) \\ & -\mathrm{i}[\mu^{z}_{\mathbf{R}}(\mu^{\rho}_{\mathbf{R}'}\cdot\mathbf{k})+\mu^{z}_{\mathbf{R}'}(\mu^{\rho}_{\mathbf{R}}\cdot\mathbf{k})]\frac{\partial D(z_{ss'})}{\partial z_{ss'}} - \mu^{z}_{\mathbf{R}}\mu^{z}_{\mathbf{R}'}\frac{\partial^2 D(z_{ss'})}{\partial z^2_{ss'}}\Big\}, \end{aligned} \tag{71}$$

with

$$D(z_{\Delta\mathbf{R}}) = \frac{1}{k}\left[\mathrm{e}^{kz}\mathrm{erfc}(\frac{k}{2\kappa}+\kappa z) + \mathrm{e}^{-kz}\mathrm{erfc}(\frac{k}{2\kappa}-\kappa z)\right], \tag{72}$$

where superscript $\rho$ labels the in-plane components and $z$ labels the out-of-plane component. And the correction term is

$$E_{\mathrm{corr}} = \frac{2\kappa\sqrt{\pi}}{L^2}\sum_{i,j=1}^{N}\mu^{z}_{\mathbf{R}}\mu^{z}_{\mathbf{R}'}\ \mathrm{e}^{-\kappa^2 z^2_{\Delta\mathbf{R}}} - \frac{2\kappa^3}{3\sqrt{\pi}}\sum_{i=1}^{N}\mu^{2}_{\mathbf{R}}. \tag{73}$$

In figure 3, we show a test for calculating DDI via EW2D and EW3D. To derive the DDI energy for the same system of *xy*-periodic and *z*-free film, EW2D can be used directly while EW3D requires extra treatment. EW3D requires a *xyz*-periodic structure, and it is done by adding a few UC vacuum. EW3D method will be fast if the vacuum is not too large, but is inaccurate due to its unconsidered layer interaction errors. When deal with in-plane polarization, EW3D reaches convergence with EW2D as quick as upon 3UC vacuum. However, EW3D shows slow convergence for out-of-plane polarization upon increasing vacuum slab thickness. Considering this, we will use EW2D for 2D calculation to ensure our results.

### 3.2.3. *Monte Carlo Calculation*

We use the aforementioned Hamiltonian with parameters derived in the last subsection. Since most energy terms of the Hamiltonian except DDI are localized, we use the single flip algorithm (each time we flip one variable). Each Monte Carlo sweep (MCS) consists of a series of trial moves of the FE modes on each site $\mathbf{u_R}$ and the homogeneous strain $\eta^{\mathrm{H}}$. Here the homogeneous strain components take 20–100 trial moves repeatedly upon the fixed FE mode in one MCS, due to the fact that the lattice strain corresponds to larger effective mass. If an unreasonable strain is accepted, several MCS will be used to correct it to a reasonable value. The repeated sampling of strain in one MCS facilitate the total sampling. The step sizes are adapted to control the accept ratio in range of 20%–30%. For each simulation configuration (cell, temperature, and external pressure), we run at least 200 000 MCSs, in which first 150 000 MCSs are used to ensure thermal equilibrium and last 50 000 MCSs are used for statistics.

The long-range nature of ferroelectricity requires large-scale simulations. Here we take the simulation cells as $10\times10\times10$ periodic supercell for bulk. It corresponds to a supercell of $a = 63.2$ Å and 8000 atoms, which means huge computation loads for DFT calculations. That's also the reason that we'd like use a model Hamiltonian method rather than *ab initio* molecular dynamics. The convergence test for this supercell has been shown in figure 4. The errors from the cell sizes are controlled to a few Kelvins, which are accurate enough to tackle the issues in [32], telling the thickness dependency of Curie temperature.

### 3.2.4. *Pressure compensation*

The lattice strain has crucial influence in FE phase transitions. Since the exact exchange correlation functional has not been found, the DFT results might be deviated from the real ones. The insufficiently accurate electronic structure of DFT, would lead to misestimation of the geometry and hence to inconsistent transition temperature. An extra pressure is used here to compensate this error. We determine this compensation pressure by comparing with the experimental results. As shown in figure 5, we calculate the phase transitions of bulk SnTe at different external pressures $p_{\mathrm{ext}}$. The FE modes stay zero at high temperatures, while they suddenly jump to finite values below the critical temperature $T_{\mathrm{c}}$ and gradually saturate. The lattice strain experience the same jump near the $T_{\mathrm{c}}$. The lattice shows contracted with decreasing temperature above $T_{\mathrm{c}}$, and turns to expanded and tilted. Therefore,

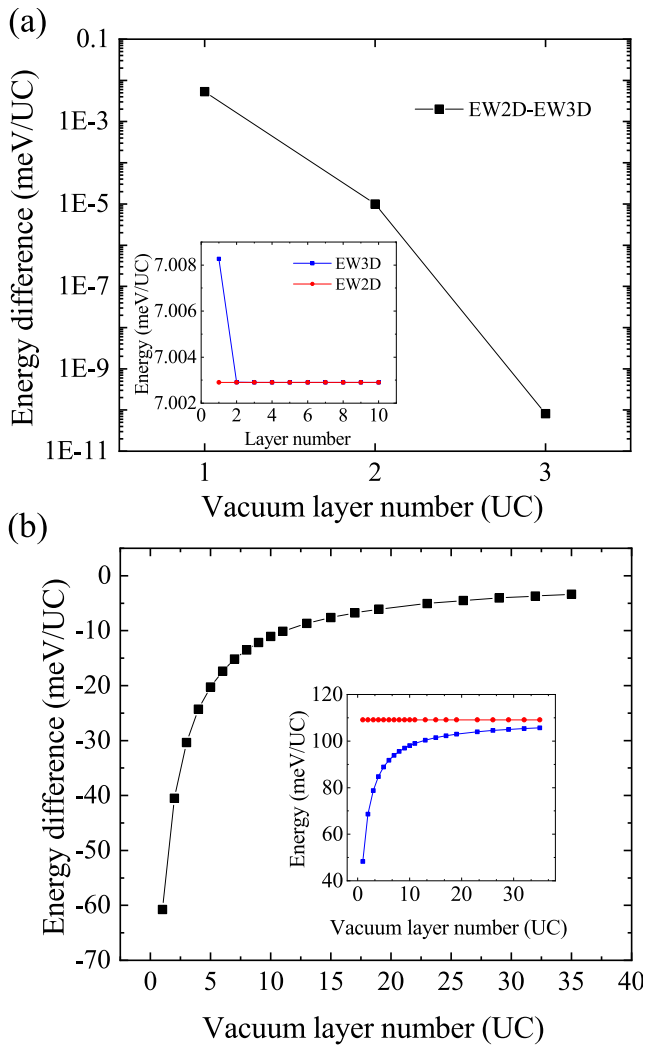


**Figure 3.** EW3D and EW2D results for $V^{(2)}_{n,long,2D}$ calculations in film geometry. (a) and (b) Shows the convergence result for in-plane polarization and the out-of-plane polarization, respectively. The insets show their absolute energy values. The typical Ewald summation is exact for 3D periodic system. Thereby for DDI in films, it can also be counted by placing the film in large enough vacuum. Our results confirm this numerically by showing that the EW3D results approach the EW2D ones when the vacuum layer is thick. In the mean time, it is also clear that in simulating a 2D system the EW2D method is much more efficient.

we obtained the pressure-temperature phase diagram of bulk SnTe (figure 6). Comparing with experimental results, we found ∼2 GPa gives reasonable $T_c$ for bulk SnTe (figure 5). This compensation pressure is reasonable in its magnitude. That is, the compensation pressure must be consistent with the feature of density functionals. As the general performance of GGA functional, SCAN functional slightly overestimate the lattice constant, requiring the compensation pressure to be positive and small. LDA, however, underestimate the lattice constant, requiring the compensation pressure to be negative and larger. This is true in our results, since BTO with LDA uses a −8 GPa compensation pressure[3], and SnTe with SCAN using a 2 GPa compensation pressure for bulk.

Though the compensation pressure can correct the lattice constant, the choice of functionals should be material-specific to better describe the phonon related properties. We tried three different levels of functionals (LDA, PBE for GGA level, and SCAN for meta-GGA level) for SnTe and found that the result of SCAN functional better reproduce the experiments. The LDA indicates no soft mode and is qualitatively incorrect, while both PBE and SCAN yield soft modes. The latter two have quantitative difference in the switch energy barrier (the energy difference between the paraelectric and ferroelectric state): PBE underestimates the barrier and SCAN gives more reasonable one. Kai *et al* also highlighted the importance of more accurate functional for SnTe [36]. For perovskites, LDA had been proven to be good enough in Vanderbilt's pioneering works [16, 28].

[3] In [16], Vanderbilt use −4.8 GPa compensation pressure in order to fit all the three transition temperature (namely C–T, T–O, O–R) in BTO. This leads to a ∼100 K divergence with experiments for Curie temperature. Here we use −8 GPa to better fit the Curie temperature (namely C–T).

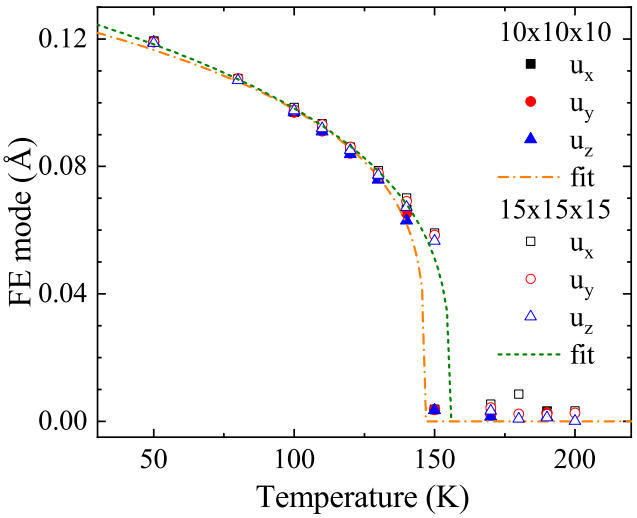


**Figure 4.** Convergence test for the simulation cell. $10 \times 10 \times 10$ supercell and $15 \times 15 \times 15$ supercell are in coincidence at low temperature and show a few deviation near the critical point. $10 \times 10 \times 10$ cell shows ~10 K difference from $15 \times 15 \times 15$ cell. In fact, this range of error is far lower than the difference between bulk and film (several hundreds of Kelvin), or among films of different layers (several tens to hundreds of Kelvins). Considering 4 times atoms and at least 16 times computation loads with the $15 \times 15 \times 15$ cell, we adopt $10 \times 10 \times 10$ cell for latter simulations.

To emphasize, when studying the thickness dependency of $T_c$ in films, threats from the large extrinsic factor of lattice strain can be ruled out by setting a same compensation pressure in our method. However, the other model methods such as Landau's phenomenological model, $\phi^4$ model, etc cannot guarantee this, since strain terms are not considered and the parameterization is done in one specific structure. One could see from the strain-temperature phase diagram in [37], $T_c$ for 1UC SnSe varies from 64 K to 640 K among different strains. This uncertainty actually hinder the exploration of the thickness dependency of $T_c$. In our effective Hamiltonian method, the built-in strain-pressure relation makes it possible to exclude extrinsic strain effect and question the intrinsic size effects of SnTe's abnormalities. Using a same extra pressure, we have show the clearly different tendency upon going from bulk to thin films in SnTe [32].

### 3.3. M-type hexaferrites

Hexaferrite exhibits the triangular lattice structure. In $BaFe_{12}O_{19}$ material of this type, it was reported to be potential 'dipole glass' upon the geometry frustration meets the quantum fluctuation [9, 38]. Previous studies have pointed out the antiferroelectric aligning tendency between NN sites via first-principles calculation [9]. However, it requires large simulation cell and path-integral simulations to concern the geometry frustration and quantum fluctuation, respectively. It's unaffordable for DFT, so that nowadays the researchers studied this material via a too rough model with only DDI included. Despite its sophisticated structure than the perovskite or the rocksalt structure, the displacive and soft phonon feature is similar with the later two structures. Regarding the adaptability, we propose that an effective Hamiltonian studies is suitable for this system and would offer physical insights.

There're two branches of the soft phonon modes, of which one is FE mode and the other is AFE mode [9]. The Bravais cell has center inverse symmetry so that he localized displacement pattern are same in one half of the cell and opposite in another half. Instead of define two local modes originated from FE and AFE respectively, we could find a smaller unit and define only one local mode. we choose to separate the cell by the half plane into two equal local units. The local mode of this unit is mainly the relative motion of the Fe centered bipyramid along the long axis. We label the local mode by a scalar $u_{\mathbf{R}}$. The sites are connected by a triangular network and the polarization of each site is either up or down. The picture differs from the spin model only for the polarizations do not exhibit a fixed value.

Upon this reconstruction into smaller local unit, the inverse symmetry for the interaction is broken. We need revisit the derivation of the Hamiltonian and subsequently consider the odd order terms. Analogous to former analysis, we obtain the effective Hamiltonian, as six terms

$$V^{\text{eff}} = V_{\text{n}}^{(1)} + V_{\text{n,short}}^{(2)} + V_{\text{n,long}}^{(2)} + V_{\text{elastic}} + V_{\text{pc}} + V_{\text{lmc}}, \tag{74}$$

where the formula for $V_{\text{elastic}}$ and $V_{\text{pc}}$ are unchanged, the other terms are changed by keeping the leading order terms up to third order (other than fourth order in previous section). They are written out as

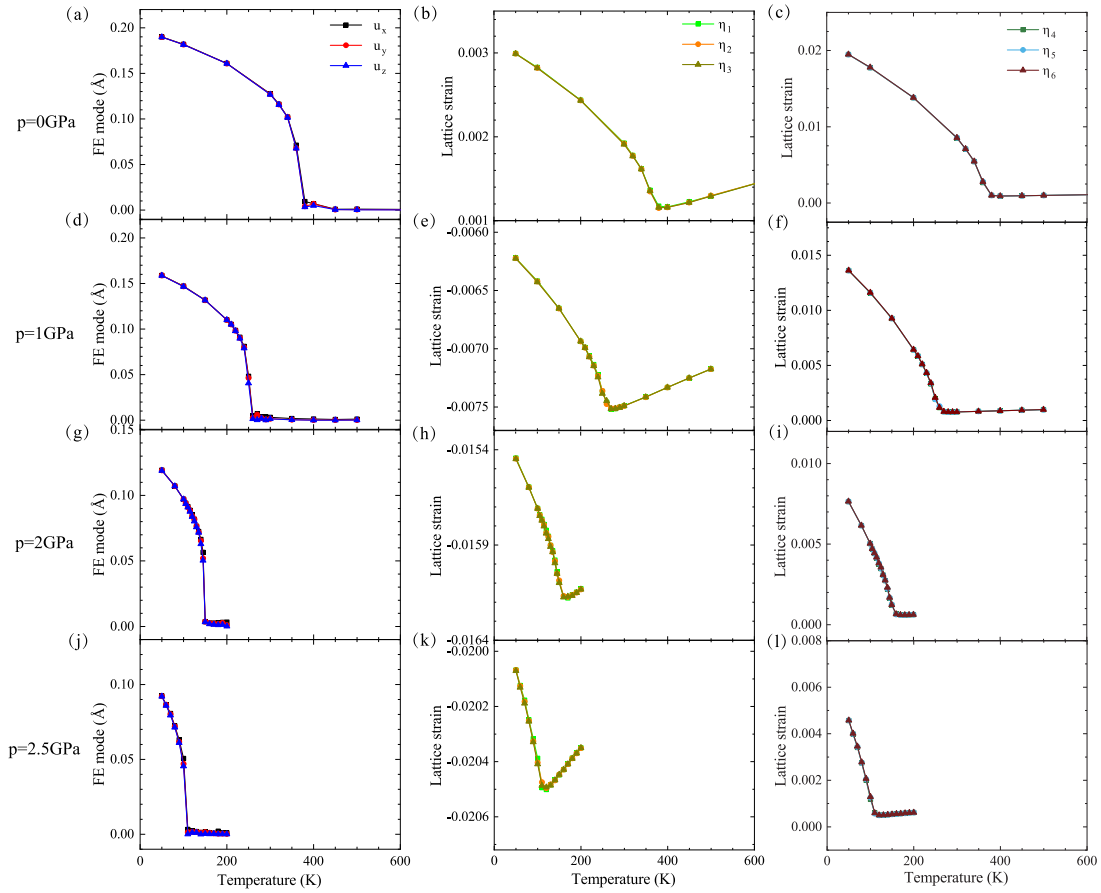


**Figure 5.** The microscopic details of the phase transitions in bulk SnTe under different pressures. (a), (d), (g) and (j) shows the magnitudes of FE modes, (b), (e), (h), (k) and (c), (f), (i) and (k) shows the magnitudes of diagonal and non-diagonal lattice strain, respectively.

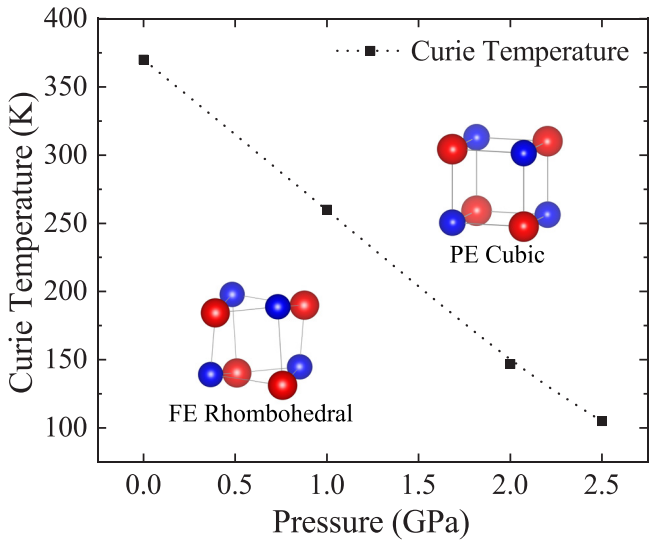


**Figure 6.** The pressure-temperature phase diagram of bulk SnTe. The compensation pressure we determined is 2 GPa for bulk SnTe, which should be shifted when comparing with the experiments. This leads to Curie temperature $T_c = 147$ K corresponding to experiments at 0 GPa, where ~50 K is left to count for the defect effects.

$$V_{\mathrm{n}}^{(1)} = \sum_{\mathbf{R}} \left[ Q^{(2)} \left( u_{\mathbf{R}} \right)^2 + Q^{(3)} \left( u_{\mathbf{R}} \right)^3 \right], \tag{75}$$

$$V_{\mathrm{n,short}}^{(2)} = \sum \sum_{|\Delta \mathbf{R}| < R_{\mathrm{cut}}} K_{\Delta \mathbf{R},uu}^{(1,1)} u_{\mathbf{R}} u_{\mathbf{R}'} \tag{76}$$

$$V^{(2)}_{\text{n,long}} = \sum\sum_{\text{FE}} \frac{\mu_{\mathbf{R}} \cdot \mu_{\mathbf{R}'} - 3\left(\mu_{\mathbf{R}} \cdot \Delta\mathbf{R}\right)\left(\mu_{\mathbf{R}'} \cdot \Delta\mathbf{R}\right)}{\epsilon\left(\Delta\mathbf{R}\right)^2} \tag{77}$$

$$V_{\text{lmc}} = \sum_{\mathbf{R}l} A_{lu}\eta_{\mathbf{R}l}u_{\mathbf{R}} + \frac{1}{2}\sum_{\mathbf{R}l} B_{luu}\eta_{\mathbf{R}l}u^2_{\mathbf{R}}. \tag{78}$$

We could carry out later investigations based on this Hamiltonian.

## 4. Perspective

In total, the phonon-related effective Hamiltonian provides to be an alternative to bruteforce *ab initio* simulations, which retains both simplicity and the predictive power of the first-principles method. Since it was proposed by Vanderbilt *et al* in 1990s, this method has shown success in predicting the FE properties in perovskites. Owning to the same displacive feature and phase transition driving by the soft modes, it can capture the essential physics for general displacive FE materials. In this manuscript, we explain the theoretical principles and some technical treatments of a self-developed implementation of this method in detail and show how it is applied in the simulations of 3D SnTe, 2D SnTe, and hexaferrite. Since the large scale simulations of high accuracy with high level DFT functionals are still not reachable for soon, we believe this method provides to be a good alternative especially for some complicated problems and systems.

## Acknowledgments

The authors are supported by the National Natural Science Foundation of China under Grant Nos. 11275008, 11422431, 11774003 and 11634001. The computational resources were supported by the High-performance Computing Platform of Peking University, China.

## ORCID iDs

Qi-Jun Ye https://orcid.org/0000-0002-9473-4915

## References

[1] Lines M E and Glass A M 2001 *Principles and Applications of Ferroelectrics and Related Materials* (Oxford: Oxford University Press)
[2] Junquera J and Ghosez P 2003 *Nature* **422** 506
[3] Spaldin N A 2004 *Science* **304** 1606
[4] Ahn C H, Rabe K M and Triscone J-M 2004 *Science* **303** 488
[5] Scott J F 2007 *Science* **315** 954
[6] Choi T, Lee S, Choi Y J, Kiryukhin V and Cheong S-W 2009 *Science* **324** 63
[7] Martin L W and Rappe A M 2016 *Nat. Rev. Mater.* **2** 16087
[8] Young S M and Rappe A M 2012 *Phys. Rev. Lett.* **109** 116601
[9] Wang P S and Xiang H J 2014 *Phys. Rev.* X **4** 011035
[10] Huang C, Du Y, Wu H, Xiang H, Deng K and Kan E 2018 *Phys. Rev. Lett.* **120** 147601
[11] Landau L D 1937 *Phys. Z. Sowjetunion* **11** 26
[12] Landau L D L E 1980 *Course of Theoretical Physics vol. 5. Statistical Physics* 3rd edn (Oxford: Pergamon) (part 1)
[13] Wojdeł J C and Íñiguez J 2014 *Phys. Rev.* B **90** 014105
[14] Paul A, Sun J, Perdew J P and Waghmare U V 2017 *Phys. Rev.* B **95** 054111
[15] Rabe K M and Joannopoulos J D 1987 *Phys. Rev.* B **36** 6631
[16] Zhong W, Vanderbilt D and Rabe K M 1995 *Phys. Rev.* B **52** 6301
[17] Bellaiche L and Vanderbilt D 2000 *Phys. Rev.* B **61** 7877
[18] Bellaiche L, Garcia A and Vanderbilt D 2000 *Phys. Rev. Lett.* **84** 5427
[19] Kornev I, Fu H and Bellaiche L 2004 *Phys. Rev. Lett.* **93** 196104
[20] Meyer B and Vanderbilt D 2002 *Phys. Rev.* B **65** 104111
[21] Nishimatsu T, Waghmare U V, Kawazoe Y and Vanderbilt D 2008 *Phys. Rev.* B **78** 104104
[22] Kornev I A *et al* 2005 *Phys. Rev. Lett.* **95** 196804
[23] Chen L *et al* 2015 *Phys. Rev. Lett.* **115** 267602
[24] Rabe K M and Waghmare U V 1992 *Ferroelectrics* **136** 147
[25] Resta R 1994 *Rev. Mod. Phys.* **66** 899
[26] King-Smith R D and Vanderbilt D 1993 *Phys. Rev.* B **47** 1651
[27] Resta R, Posternak M and Baldereschi A 1993 *Phys. Rev. Lett.* **70** 1010
[28] Zhong W, Vanderbilt D and Rabe K M 1994 *Phys. Rev. Lett.* **73** 1861
[29] Rabe K M and Waghmare U V 1995 *Phys. Rev.* B **52** 13236
[30] Íñiguez J, García A and Pérez-Mato J M 2000 *Phys. Rev.* B **61** 3127
[31] Chang K *et al* 2016 *Science* **353** 274

[32] Ye Q-J, Liu Z-Y, Feng Y, Gao P and Li X-Z 2018 *Phys. Rev. Lett.* **121** 135702
[33] Allen M P and Tildesley D J 2017 *Computer Simulation of Liquids* vol 1 (Oxford: Oxford University Press) p 267
[34] Almahmoud E, Navtsenya Y, Kornev I, Fu H and Bellaiche L 2004 *Phys. Rev.* B **70** 220102
[35] Grzybowski A and Bródka A 2002 *Chem. Phys. Lett.* **361** 329
[36] Liu K *et al* 2018 *Phys. Rev. Lett.* **121** 027601
[37] Fei R, Kang W and Yang L 2016 *Phys. Rev. Lett.* **117** 097601
[38] Shen S-P *et al* 2016 *Nat. Commun.* **7** 10569